OXFORD

Cryptic splice mutation in the fumarate hydratase gene in patients with clinical manifestations of Hereditary Leiomyomatosis and Renal Cell Cancer

Daniel R. Crooks[1], Geetha Mariah Cawthon[1], Christina M. Fitzsimmons[2], Minervo Perez[3], Christopher J. Ricketts[1], Cathy D. Vocke[1],

Ye Yang[1], Lindsay Middelton[1], Debbie Nielsen[1], Laura S. Schmidt[1,4], Mayank Tandon[5], Maria J. Merino[6], Mark W. Ball[1],

Jordan L. Meier[3], Pedro J. Batista[2], William Marston Linehan [ID][1,*]

[1]Urologic Oncology Branch, Center for Cancer Research, National Cancer Institute, 10 Center Drive, Bethesda, MD 20892, United States
[2]RNA Metabolism and Epitranscriptomics Unit, Laboratory of Cell Biology, Center for Cancer Research, National Cancer Institute, 9000 Rockville Pike, Bethesda, MD 20892, United States
[3]Chemical Biology Laboratory, National Cancer Institute, 1050 Boyles St., Frederick, MD 21072, United States
[4]Basic Science Program, Frederick National Laboratory for Cancer Research, 1050 Boyles St. Frederick, MD 21701, United States
[5]CCR Collaborative Bioinformatics Resource (CCBR), Frederick National Laboratory for Cancer Research, Leidos Biomedical Research, Inc., 1050 Boyles St., Frederick, MD 21072, United States
[6]Translational Surgical Pathology, Laboratory of Pathology Center for Cancer Research, National Cancer Institute, National Institutes of Health, 10 Center Drive, Bethesda, MD 20892, United States
*Corresponding author. Urologic Oncology Branch, Center for Cancer Research, National Cancer Institute, 10 Center Drive, Room 1W-5940, Bethesda, MD 20892, USA. E-mail: WML@nih.gov

Abstract

Hereditary leiomyomatosis and renal cell carcinoma (HLRCC) is an autosomal dominant condition characterized by the development of cutaneous and uterine leiomyomas and risk for development of an aggressive form of papillary renal cell cancer. HLRCC is caused by germline inactivating pathogenic variants in the fumarate hydratase (*FH*) gene, which encodes the enzyme that catalyzes the interconversion of fumarate and L-malate. We utilized enzyme and protein mobility assays to evaluate the FH enzyme in a cohort of patients who showed clinical manifestations of HLRCC but were negative for known pathogenic *FH* gene variants. FH enzyme activity and protein levels were decreased by 50% or greater in three family members, despite normal *FH* mRNA expression levels as measured by quantitative PCR. Direct Nanopore RNA sequencing demonstrated 57 base pairs of retained intron sequence between exons 9 and 10 of polyadenylated *FH* mRNA in these patients, resulting in a truncated FH protein. Genomic sequencing revealed a heterozygous intronic alteration of the *FH* gene (chr1: 241498239 T/C) resulting in formation of a splice acceptor site near a polypyrimidine tract, and a uterine fibroid obtained from a patient showed loss of heterozygosity at this site. The same intronic *FH* variant was identified in an unrelated patient who also showed a clinical phenotype of HLRCC. These data demonstrate that careful clinical assessment as well as biochemical characterization of FH enzyme activity, protein expression, direct RNA sequencing, and genomic DNA sequencing of patient-derived cells can identify pathogenic variants outside of the protein coding regions of the *FH* gene.

Keywords: renal cell carcinoma; hereditary leiomyomatosis and renal cell cancer; cryptic splice site; hereditary diseases

Introduction

Patients with hereditary leiomyomatosis and renal cell carcinoma (HLRCC) are predisposed for the development of smooth muscle cutaneous and uterine leiomyomas. Individuals with HLRCC are also at risk for the development of an aggressive form of Type 2 papillary renal cell cancer (RCC) that has the potential to spread when the primary tumor is small (1). The estimated cumulative risk for development of renal cancer in HLRCC patients is 15%, and renal tumors have occurred in individuals as young as 10 years of age (2). The aggressive and infiltrative nature of HLRCC-related RCC tumors has led to the recommendation that individuals with genetically confirmed HLRCC should undergo annual abdominal imaging for surveillance of renal manifestations starting at 8 years of age (2). Additionally, early surgical intervention with wide

surgical margins and consideration of retroperitoneal lymph node dissection is recommended for HLRCC patients manifesting with renal lesions (1).

HLRCC is caused by germline heterozygous inactivating mutations in the fumarate hydratase (*FH*) gene, which encodes the FH enzyme that catalyzes the interconversion of fumarate and L-malate in the Krebs cycle. HLRCC patients harboring *FH* mutations in their germline show diminished FH enzyme activity levels in cultured patient dermal fibroblasts and lymphocytes, typically at levels of 50% or less than controls (3,4). FH-deficient tumors exhibit complete loss of FH enzyme activity in the affected tumor cells and accumulate high levels of fumarate (5). This leads to a pseudohypoxia phenotype characterized by stabilization of HIF1α (6) and inhibition of α-ketoglutarate-dependent

dioxygenases resulting in hypermethylation of DNA and histones (7–9). Accumulation of fumarate in FH-deficient tumors is also associated with the non-enzymatic covalent modification of cysteine residues in proteins leading to the formation of an S-(2-succinyl)-cysteine (2-SC) protein adduct. This modification known as succination inactivates multiple proteins resulting in modulation of tumor biology and metabolism (10,11). Additionally, succination inactivates the mitochondrial nucleoid components responsible for the maintenance and replication of mitochondrial DNA resulting in copy loss and mutation of mtDNA in FH-deficient tumors (12). The 2-SC protein adduct in FH-deficient cells and tumors can be detected by histochemical and proteomic methodologies (10,13,14), and positive 2-SC immunoreactivity in tumor cells is increasingly used as a tool to facilitate diagnosis of FH-deficient RCC (15–17).

Screening for HLRCC in patients and their families involves obtaining a detailed family history as well as careful clinical evaluation of patients for manifestations of uterine leiomyomata, cutaneous leiomyomas, and renal lesions. Clinical diagnosis includes germline DNA sequencing of the *FH* gene, performed by a qualified Clinical Laboratory Improvement Amendments (CLIA)-approved laboratory. The *FH* gene is evaluated for missense, frameshift, and nonsense mutations in the exon sequences, and intronic sequences very near the exon boundaries are evaluated for splice site mutations (3). In this manner, 31 pathogenic *FH* variants were identified in 56 families with manifestations of HLRCC, with an overall detection rate of over 90% (3). Next-generation techniques have facilitated the identification of germline heterozygous large-scale deletions of the *FH* gene in additional individuals presenting with clinical manifestations of HLRCC (18,19).

Despite the relatively high detection rate for HLRCC using the standard genetic screening procedures outlined above, pathogenic alterations in the *FH* gene may remain undetected in some patients and their families since large-scale chromosomal rearrangements, promoter alterations, and deep intronic variants are not typically evaluated using the standard screening techniques. In this study, we utilized enzymatic activity assays to evaluate *FH* activity in material from patients with clinical manifestations of HLRCC who lacked standard CLIA-identifiable variants in the *FH* gene. By comparing enzymatic activity, protein expression and mobility, and mRNA expression of the *FH* gene in cultured dermal fibroblast and lymphoblast cell lines obtained from these individuals, we identified a discrepancy between FH protein and mRNA levels. Direct RNA sequencing of patient-derived mRNA transcripts identified retained intronic sequences, consistent with aberrantly spliced *FH* mRNA. Finally, genomic DNA sequencing confirmed the presence of a novel deep intronic point mutation resulting in the creation of a novel splice acceptor site near a polypyrimidine tract. Together, these data demonstrate the clinical utility of evaluating FH activity and mRNA expression in cells obtained from patients suspected of having HLRCC but lacking a detectable sequence variant in the *FH* coding region.

Materials and methods
Patients and patient-derived primary cells
Patients were evaluated and treated at the Clinical Center of the National Institutes of Health on Urologic Oncology Branch, National Cancer Institute protocols (NCI-97-C-0147 and NCI-03-C-0066) approved by the NCI Institutional Review Board, and written informed consent was given for participation in this study.

Patents were tested for germline mutations in the *FH* gene by CLIA-certified genetic testing. Dermal fibroblast cultures were obtained from dermal biopsy explants maintained on tissue culture dishes in a humidified incubator at 37 °C in the presence of 5% O_2 and 5% CO_2 and propagated in DMEM medium containing 5 mM D-glucose, 4 mM glutamine, 1 mM pyruvate, 25 mM HEPES, 10% fetal bovine serum (FBS), 100 units/ml of penicillin and streptomycin, and 0.25 μg/ml amphotericin-B. All experiments were performed on fibroblast cultures at passages 3–6. Immortalized lymphoblastoid B cell lines were generated by EBV transformation of blood lymphocytes and were cultured in RPMI 1640 medium supplemented with 1 mM pyruvate, 4 mM glutamine, 10% FBS and 100 units/ml of penicillin and streptomycin, 0.25 μg/ml amphotericin-B (all reagents from Gibco, Thermo Fisher Scientific Inc., MA, USA).

In-gel enzyme activity assays
FH and malic NAD + -reductase enzyme activities were separated by native gel electrophoresis using pre-cast 1 mm 7% Tris-acetate polyacrylamide gels (Invitrogen, CA, USA). Briefly, whole cell lysates were prepared on ice by sonication in lysis buffer consisting of 10 mM Tris, pH 8.0, 0.1% Triton X-100, 3 mM KCl, 3 mM $MgCl_2$, 3 mM sodium citrate, and protease inhibitors (Complete™ EDTA-free, Roche), followed by centrifugation at 21 000× g for 30′ at 4 °C. Protein concentration of the recovered supernatants was measured by BCA assay and 10 μg of total cellular protein was loaded into the gel, and the samples were subjected to electrophoresis at 4 °C for 2 h at 125 V, with running buffer consisting of 25 mM Tris, 192 mM glycine. For measurement of FH activity, the gels were immersed in 10 ml of a solution pre-warmed to 37 °C, consisting of 100 mM Tris, pH 7.4, 1 mg/ml 3-(4,5-dimethylthiazol-2-yl)-2,5-diphenyltetrazolium bromide (MTT), 1 mM NAD+, 0.184 mg/ml phenazine methosulfate (PMS), 150 units of porcine heart malic dehydrogenase (Sigma-Aldrich), and 5 mM Na fumarate. The gels were gently rocked at 37 °C in the dark for 5–10 min, until FH enzyme activity bands were developed, at which point the gels were de-stained in the dark with sequential incubations in de-ionized water until the background was clear, and the gels were scanned immediately using a transmitted light flatbed scanner. NAD-malate dehydrogenase enzyme activity was assessed by incubation of duplicate gels with 100 mM Tris, pH 7.4, 1 mg/ml iodonitrotetrazolium bromide (INT), 1 mM NAD+, 0.184 mg/ml phenazine methosulfate (PMS), and 5 mM Na L-malate.

Fluorogenic FH activity assay
Whole cell proteomes were extracted from patient samples by sonication. Briefly, 100 μl of lysis buffer containing ice-cold PBS, protease inhibitor cocktail (1X, EDTA-free, Cell signaling #5871S) and phenylmethylsulfonyl fluoride (1 mM Sigma #78830), was added to each sample. Samples were then incubated on ice in preparation for sonication. Each sample was sonicated on ice using a 100 W QSonica Q700 sonicator (10 × 3-s pulses, amplitude 1, 30 s resting in between pulses) equipped with microtip #4417. Following sonication, lysates were pelleted by centrifugation (20 000 relative centrifugal force × 30 min, 4 °C) to discard insoluble cellular debris and the supernatant were recovered for protein concentration measurement on a Qubit 2.0 Fluorometer using a Qubit Protein Assay Kit. Lysates were diluted to a 2 mg/ml concentration and stored at −80 °C for FH enzyme activity assay.

To determine FH activity, proteomes (5 μg) were incubated with neutralized L-malic acid (25 mM) and sodium phosphate

buffer (100 mM, pH 7) in a final reaction volume of 100 μl in a UV-Star 96-well plate (Greiner Bio-One #655801). Plates were covered with sealing film (Eppendorf #0030127781) and incubated at 37°C for 2 h. Following incubation, 100 μl of tetrazole 1 (300 μM in acetonitrile, final reaction concentration of 150 μM) was added to each well and mixed by pipetting then irradiated with 302-nm light for 2 min. Samples were then transferred to a black clear-bottom 96-well plate (Greiner Bio-One #655090), and fluorescence measurements were taken on a BioTek Cytation5 plate reader controlled by Gen5 detection software (version 3.09). Measurements were taken by using an excitation wavelength of 410 nm, and a spectral scan was performed to monitor emission wavelengths between 430 and 630 nm by 5-nm increments. To determine FH activity in patient samples, a fumarate standard curve was generated using 0, 25, 50, 100, 200, 400, and 800 μM concentrations in 100-mM sodium phosphate buffer (pH 7) in a final volume of 100 μl. Following addition of tetrazole (300 μM in acetonitrile, final reaction concentration of 150 μM) to the fumarate standards, samples were subjected to irradiation and fluorescence measurements were taken as described above. Spectral measurements were plotted using GraphPad Prism 9 software (version 9.1) and a smooth of curve function was used to generate area under the curve (AUC) values for all samples. A simple linear regression function was fitted to the AUC values of the fumarate standards to determine the production of fumarate in the patient samples. Patient sample measurements were taken in quadruplicate technical replicates, while standard curve samples were performed in duplicate. Tetrazole 1 was synthesized as previously described (20).

Nanopore library preparation and bioinformatic processing

Cultured dermal fibroblasts from an affected patient and negative-control fibroblasts obtained from a patient affected with von Hippel Lindau disease were collected in Trizol, and total RNA was isolated following the manufacturer's protocol (Invitrogen, CA, USA). Total RNA underwent two rounds of polyA selection using NEB oligodT beads and protocol (New England Biolabs S1419S). PolyA quality was assessed by Agilent High Sensitivity RNA ScreenTape Assay. PolyA RNA (750 ng) was prepared for nanopore direct RNA sequencing following the Oxford Nanopore Technology (ONT) SQK-RNA002 kit protocol, including the optional reverse transcription step recommended by ONT. RNA sequencing on the MinION was performed using ONT R9.4 flow cells and the standard MinIT protocol script for 60 h. Data quality control was performed using MinION QC (v. 1.4.1) (21). Raw fast5 files were basecalled using Guppy (v3.5.4) and mapped to Human GRCh38.p12. genome using minimap2 (v 1.7) in splice-aware RNA mapping mode with a kmer size of 14 (*minimap2 -ax splice -uf -k14*). SAM and BAM file manipulations were performed with samtools (v 1.9), and mapped data was visualized in the Integrated Genome Viewer (IGV-2.8.0) (Broad Institute) (22). The code for nanopore processing and figure generation is available at https://github.com/BatistaLab/Exon9A_Nanopore.

Whole genome sequencing

Germline variant analysis was performed as described in Ricketts *et al.* (23), using the hg38 reference genome.

Immunohistochemistry

Five-micron thick formalin-fixed paraffin-embedded sections were cut from surgical material obtained from a myomectomy as well as from a biopsy of a dermal leiomyoma lesion. IHC staining was performed by VitroVivo Biotech (Rockville, MD) using standardized methodologies, using either anti-FH (Santa Cruz Biotechnology; 1:1000) or anti-2-succinocysteine (2SC) (Cambridge Research Biochemicals; 1:5000). Images were captured using an AxioScan.Z1 Slide Scanner (Zeiss, Oberkochen, DE).

Data access

Sequencing data will be made available by request on dbGaP (https://www.ncbi.nlm.nih.gov/gap/).

Results

Families evaluated in this study

Family 1

Patient #1 presented with biopsy-proven cutaneous leiomyomas consisting of light tan-to-brown papules present on the left posterior shoulder, right lumbar back, and central chest. This patient also had symptomatic uterine leiomyomas and underwent a total hysterectomy at an outside institution at age 33 (Fig. 1, Family #1). Patient #2, the sister of Patient #1, also presented with biopsy-proven cutaneous leiomyomas as well as symptomatic uterine leiomyomas for which she underwent a total hysterectomy at an outside institution at age 30. Patient #3, the daughter of Patient #1, presented with biopsy-proven cutaneous leiomyomas and underwent a total hysterectomy at an outside institution at age 35. All three patients were tested for pathogenic germline variants in the *FH* gene using CLIA-certified Sanger sequencing platforms; Patient #1 underwent additional deletion/duplication testing of the *FH* gene as well as karyotype analysis to rule out germline translocations involving chromosome 1. None of these tests identified a known pathogenic alteration of the *FH* gene. Several other family members in the paternal lineage were reported to have cutaneous and/or uterine leiomyomas, and a paternal uncle was reported to have RCC of undefined histology (Fig. 1, Family #1).

Family 2

Patient #4 presented with a history of uterine leiomyomas and underwent a myomectomy at an outside institution at age 30 for the removal of fibroids, the largest of which was 10 cm in diameter. Histological evaluation at the NIH Clinical Center revealed high cellularity and nuclear atypia. The patient reported dermal lesions on the right lower leg that were sensitive to touch and cold, which were confirmed to be leiomyomas upon biopsy at the NIH Clinical Center. Sequencing and deletion/duplication analysis did not reveal germline alterations in the *FH* gene, and the patient's karyotype was normal. The patient reported that two paternal aunts had a history of uterine fibroids (Fig. 1, Family #2).

In-gel activity measurement of FH enzyme activity and protein mobility in HLRCC patient-derived primary cells

In order to evaluate the functional effect of *FH* mutations on the activity and assembly of FH protein, we developed a tetrazolium-based in-gel electrophoretic FH activity assay using tris-acetate polyacrylamide gels ((12); see Materials and Methods). Concomitantly, we ran a replicate tris-acetate native gel loaded identically and electroblotted the resolved proteins onto a nitrocellulose membrane, followed by immunoblotting using a monoclonal antibody raised against FH. We evaluated FH enzyme activity and
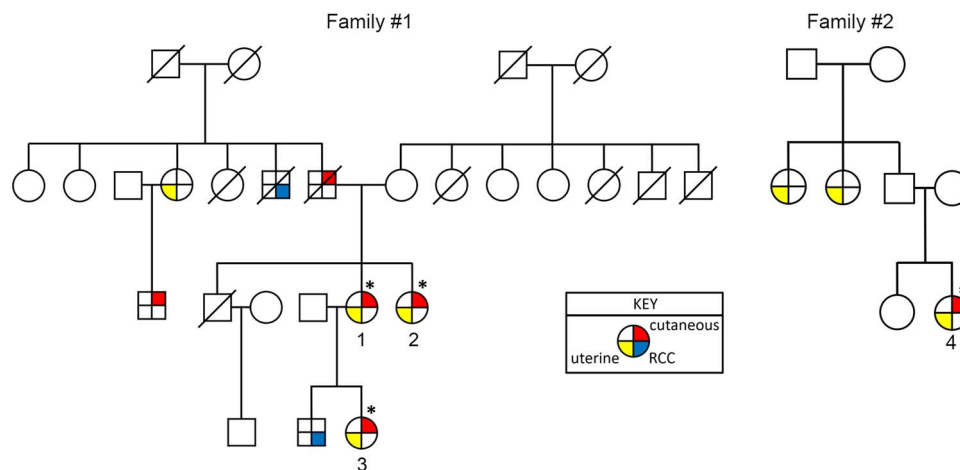
Figure 1. Pedigree of affected family members. Clinical phenotypes are denoted in colors; Red: cutaneous leiomyomata. Blue: renal cell carcinoma. Yellow: uterine leiomyomata. Asterisk (*) indicates that CLIA-certified genetic testing for *FH* mutation was performed and yielded negative results for Patients #1–4.

native gel mobility in cultured dermal fibroblasts obtained from an unaffected control patient as well as genetically confirmed HLRCC patients harboring FH variants R233H, H318Y, M454X, and L244R or complete *FH* deletion (Supplementary Material, Fig. S1A and B). All patient samples harboring *FH* missense variants exhibited a shift in the mobility of their FH enzyme activity as well as altered FH protein mobility as assessed by native FH immunoblot (Supplementary Material, Fig. S1A and B). In contrast, the patient sample harboring the FH deletion showed unaltered mobility but decreased activity and expression of the FH protein (Supplementary Material, Fig. S1A and B). Together, these data demonstrate that evaluation of native FH activity and protein expression can reveal diminished FH activity and altered FH protein mobility in HLRCC patient-derived primary cells.

Analysis of FH enzyme activity in HLRCC-phenotypic patients

Using the methodologies outlined above, we next investigated FH enzyme activity and protein expression in dermal fibroblasts and immortalized B lymphoblasts derived from our HLRCC-phenotypic patients. Using the in-gel FH activity assay, we found that FH activity was diminished in cultured fibroblasts obtained from Patients #1 and #2 as well as in fibroblasts obtained from a known HLRCC patient harboring a R343X FH variant, relative to fibroblasts obtained from a patient unaffected by HLRCC (Fig. 2A, upper panel). Native immunoblot of FH demonstrated decreased FH protein expression in the absence of a notable shift in FH protein mobility (Fig. 2A, middle panel). In contrast, malate dehydrogenase (MDH) enzyme activity, assessed as a "housekeeping" enzyme in these analyses, was similar across all four samples (Fig. 2A, lower panel).

We also evaluated FH and MDH enzyme activities in lymphoblasts obtained from each of three patients from Family #1 and compared these with a known HLRCC patient harboring a heterozygous truncating K447X variant in the FH protein, as well as with two unaffected control patients (Fig. 2B). Lymphoblasts from all three patients from Family #1 as well as the known HLRCC patient exhibited reduced FH enzyme activity (Fig. 2B, upper panel), whereas MDH activity was similar across all samples (Fig. 2B, lower panel). Notably, native FH immunoblots also revealed diminished FH levels and an absence of change in FH protein mobility in the lymphoblasts from the three

unknown patients, while the cells harboring the K477X FH variant showed evidence for an upward shift in mobility suggesting altered characteristics of the FH multimer in these cells (Fig. 2B; middle panel).

Next, FH and MDH in-gel enzyme assays were performed in triplicate dermal fibroblast samples and analyzed by densitometry to obtain a quantitative assessment of the reduction in FH enzyme activity in our patients. As compared with three patients confirmed to be unaffected by HLRCC, fibroblast FH activity was significantly reduced in a known HLRCC patient and was similarly and significantly decreased in Patients #1 and #2 (Fig. 2C). In contrast, MDH activity was not significantly different between any of the fibroblast samples evaluated (Fig. 2C). To obtain an orthogonal assessment of FH enzyme activity in our patient fibroblasts, we employed a recently described fluorogenic FH activity assay that employs the conjugation of hydrazonyl chlorides and diaryl tetrazole to create a nitrileimine intermediate that reacts with fumarate to form a fluorescent pyrazolidine cycloadduct (20,24). This assay, which measures the quantity of fumarate produced from malate during a fixed incubation period, is inherently more quantitative than the densitometry-based native gel activity assay (Supplementary Material, Fig. S2). Using the fluorogenic assay, we observed a >50% decrease in the amount of fumarate produced in fibroblast lysates obtained from Patients #1 and #2 (Fig. 2D). Fumarate production was similarly diminished in fibroblasts from a known HLRCC patient harboring a Q439P FH variant (Fig. 2D). In summary, two complementary FH enzyme assays demonstrated diminished levels of FH enzyme activity in our patients showing clinical manifestations of HLRCC in the absence of detectable *FH* gene mutations.

Analysis of FH protein levels in HLRCC-phenotypic patients

Given the unknown reason for diminished FH enzyme activity in our cohort of HLRCC-phenotypic patients, we next set out to investigate FH protein expression levels in patient-derived cells. We performed SDS-PAGE western blots to evaluate FH protein expression and found that FH protein levels were diminished in cultured fibroblasts obtained from Patients #1 and #2 as well as in an HLRCC patient harboring the R343X FH variant, relative to fibroblasts obtained from a patient unaffected by
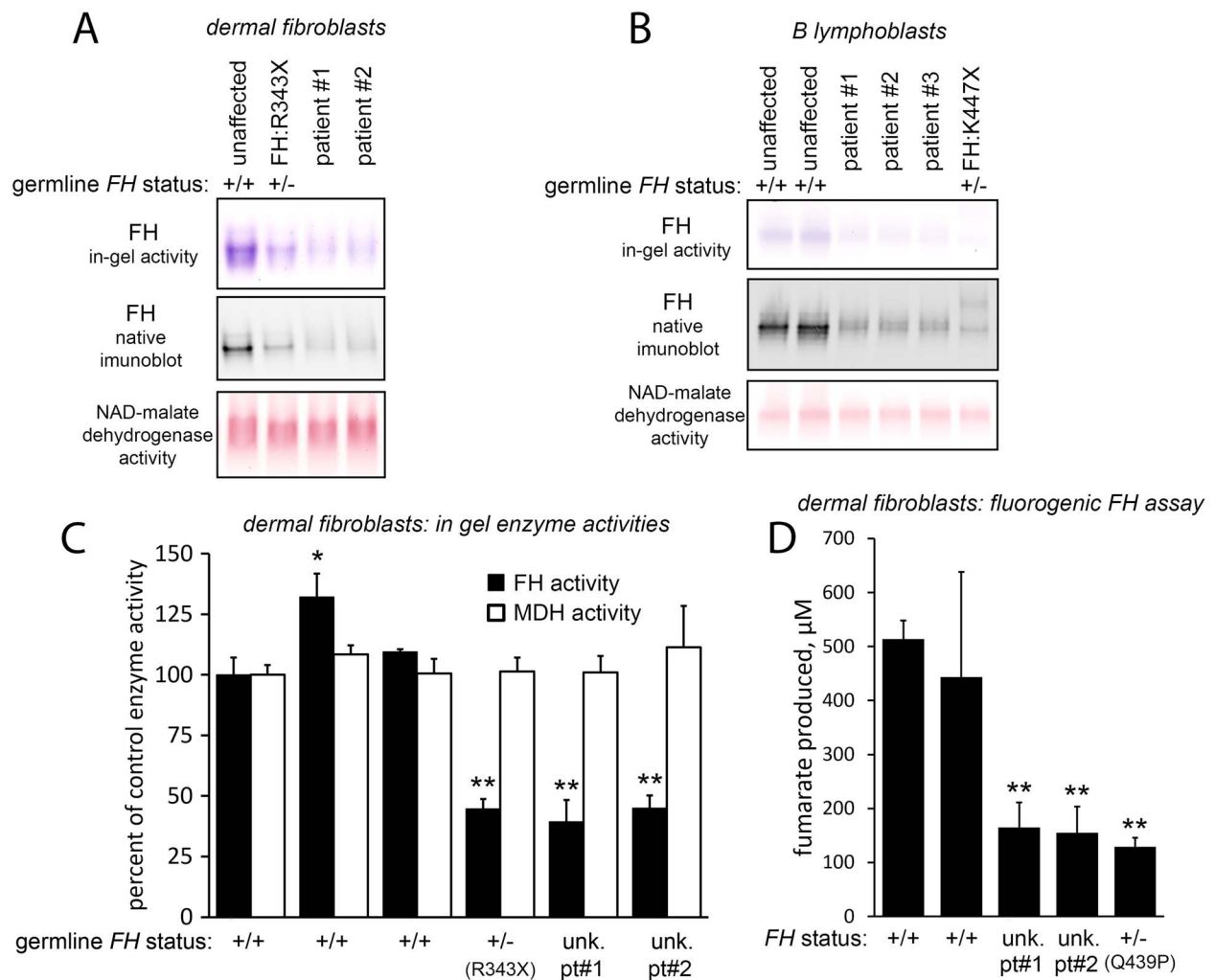
Figure 2. Analysis of FH enzyme activity in HLRCC-phenotypic patients. (**A**) Fumarate hydratase and malate dehydrogenase in-gel enzyme activity and FH protein mobility were assessed in cultured primary dermal fibroblasts obtained from a patient unaffected with HLRCC, a known HLRCC patient with a truncating R343X *FH* mutation, and Patients #1 and #2. (**B**) FH and MDH in-gel enzyme activity and FH protein mobility were assessed in cultured lymphoblasts derived from two unaffected patients, three HLRCC-phenotypic patients, and an HLRCC patient harboring a K447X *FH* mutation. (**C**) Quantitation of FH and MDH enzyme activities was performed on triplicate fibroblast cultures obtained from three unaffected individuals *(FH^{+/+})*, a known HLRCC patient *(FH^{+/−})* with a truncating R343X *FH* mutation, and Patients #1 and #2. (**D**) Fluorogenic fumarase assay was performed on fibroblast cultures obtained from two unaffected individuals *(FH^{+/+})*, a known HLRCC patient *(FH^{+/−})* with a Q439P *FH* point mutation, and Patients #1 and #2 ($n = 4$ cell pellets per patient). $*P < .05$, $**P < .01$.

HLRCC (green bands; Fig. 3A). Immunoblotting of MDH1 protein revealed comparable MDH1 protein levels in all four samples. Similar results were obtained in cultured lymphoblasts obtained from Patients #1–3, where FH protein levels were diminished in the three unknown patients as well as in an HLRCC patient harboring a K477X FH variant, as compared with two non-HLRCC controls (Fig. 3B). We repeated our SDS-PAGE protein analyses of FH and MDH1 protein levels in independent triplicate fibroblast cultures and found that FH protein levels were significantly decreased by ~50% in Patients #1 and #2 as well as in a patient harboring a truncating R343X FH variant, as compared with three control patients unaffected by HLRCC (Fig. 3C).

Analysis of *FH* mRNA in HLRCC-phenotypic patients

The enzyme activity and protein expression analyses described above indicate that somatic cells derived from normal tissues of the HLRCC-phenotypic patients exhibit diminished FH enzyme

activity and express only ~50% FH protein levels relative to controls. This suggested that an as-yet undetected alteration in the *FH* gene sequence results in loss of FH protein expression. One possibility is that an intronic mutation could alter splicing and render mRNA transcripts produced from the mutant *FH* allele susceptible to nonsense-mediated decay. To test this hypothesis, we performed quantitative PCR (qPCR) to assess total cellular *FH* mRNA levels. We found that fibroblasts derived from Patients #1 and #2 showed levels of *FH* mRNA that were comparable to two control patients unaffected by HLRCC (Fig. 4A). In contrast, mRNA levels in two HLRCC patients harboring point mutations in the *FH* gene resulting in premature stop codons (R343X and A101X) showed *FH* mRNA levels that were ~50% of control (Fig. 4A), suggesting that these truncating FH mutations result in NMD of mRNA transcripts produced from the affected *FH* alleles. Finally, UOK348 cells that harbor both a point mutation resulting in a premature stop codon (K371X) as well as an *FH* exon 5 frameshift mutation (F191LfsX11) possessed nearly undetectable *FH* mRNA levels, suggesting nearly complete NMD of all mutant cellular *FH*
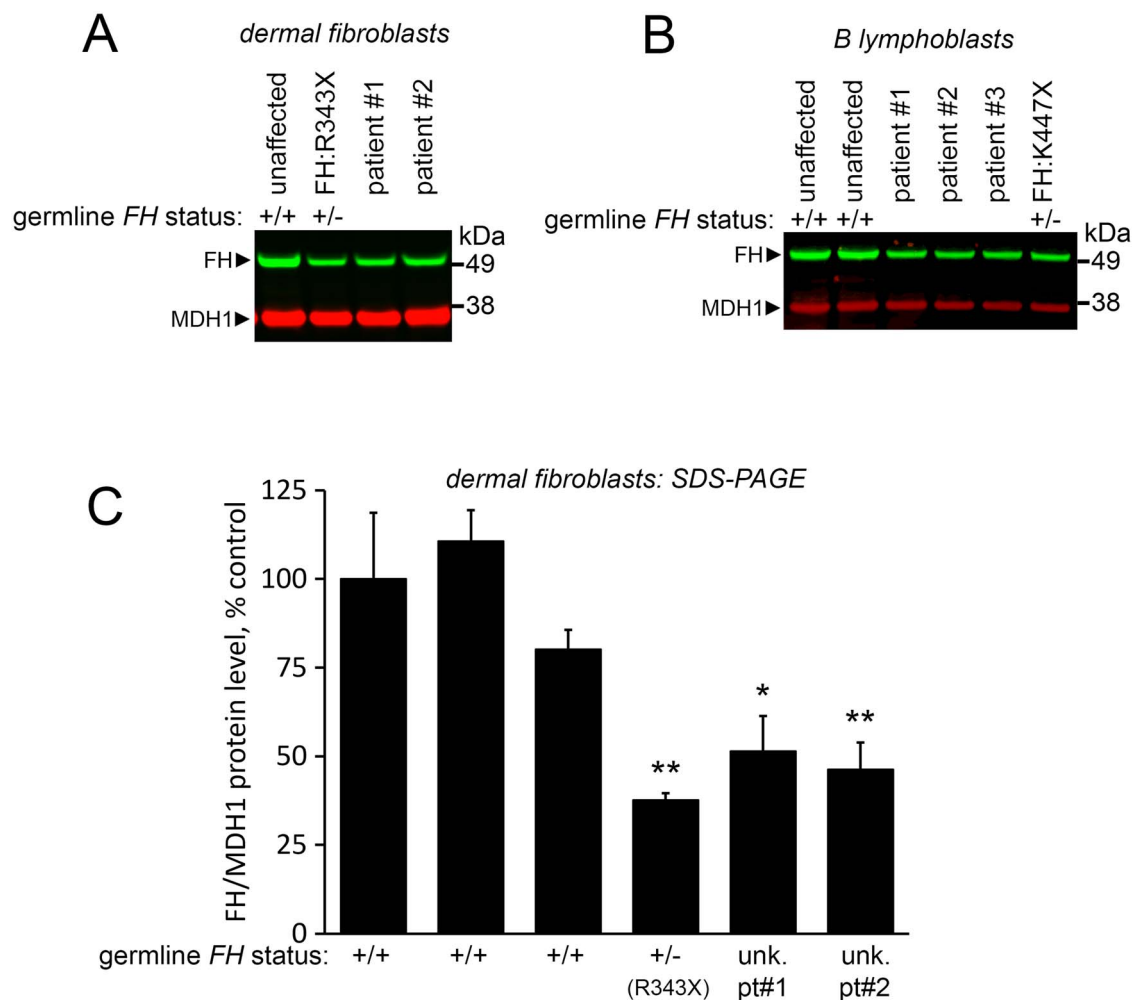
Figure 3. Analysis of FH protein expression in HLRCC-phenotypic patients. (**A**) Fumarate hydratase and malate dehydrogenase 1 protein expression was assessed in cultured primary dermal fibroblasts obtained from a patient unaffected with HLRCC, a known HLRCC patient with a truncating R343X *FH* mutation, and Patients #1 and #2. (**B**) Fumarate hydratase and malate dehydrogenase 1 protein expression was assessed in cultured lymphoblasts derived from two unaffected patients, the three HLRCC-phenotypic patients, and an HLRCC patient harboring a K447X *FH* mutation. (**C**) FH protein bands were quantified and normalized to MDH1 bands in triplicate fibroblast cultures obtained from three unaffected individuals (*FH*$^{+/+}$), a known HLRCC patient (*FH*$^{+/+}$) with a truncating R343X *FH* mutation, and Patients #1 and #2. *$P < .05$, **$P < .01$.

mRNAs. Together, these data suggested that normal cells obtained from the HLRCC-phenotypic patients produce stable *FH* mRNA transcripts from both *FH* alleles, but that the *FH* mRNA produced from one of the *FH* alleles must not produce stable or functional FH protein.

To focus on the altered *FH* mRNA allele present in the HLRCC-phenotypic patient cells, we performed long-read direct mRNA sequencing of poly-A-selected total cellular mRNA using Nanopore technology. In addition to the canonical *FH* transcript, Nanopore analysis of the *FH* mRNA sequences revealed the presence of a novel *FH* mRNA isoform containing additional sequence derived from intron 9 (Fig. 4B). Nanopore direct mRNA sequencing detected 96 and 74 *FH* mRNA reads in two independent runs in RNA obtained from an unaffected patient, all showing proper splicing between *FH* exons 9 and 10 and no *FH* mRNA reads with inclusion of cryptic exon 9A. For two independent Nanopore runs with mRNA obtained from Patient #2, we observed 27 and 28 reads with proper splicing between exons 9 and 10, and 20 and 28 *FH* mRNA reads showing inclusion of exon 9A (Fig. 4B), suggesting that this alternatively spliced *FH* allele is expressed at comparable levels to the wild-type *FH* allele.

This observation was further confirmed by RT-PCR with primers flanking exon 9 and 10, performed on cDNA prepared from all three patients from Family #1 as well as from Patient #4 from Family #2 (Fig. 4C), consistent with the presence of a new exon in the *FH* mRNA in these patients' cells.

Analysis of whole genome data obtained from blood DNA of the HLRCC-phenotypic patients revealed a single point mutation, 1:241498239 T/C, present within *FH* intron 9 (Supplementary Material, Fig. S3). Cosegregation analysis revealed that this intronic 1:241498239 T/C *FH* variant was not present in the 1000 Genomes database, despite its presence in members of both families (Supplementary Material, Fig. S3). Sanger sequencing of cDNA generated from patient cells confirmed that splicing occurs at the site of mutation. Furthermore, sequence analysis identified an AGAG motif at a new putative splice donor site that delineates the 3′ end of the new *FH* exon 9A in these patients (Fig. 4D and E). The insertion of this new exon disrupts the protein reading frame and, when included, results in a truncated version of FH protein that is 37 residues shorter than the wild-type FH protein and creates a new c-terminus (Fig. 4D and E). Thus, in these patients an intronic mutation creates a new splice acceptor site, and a splice donor site
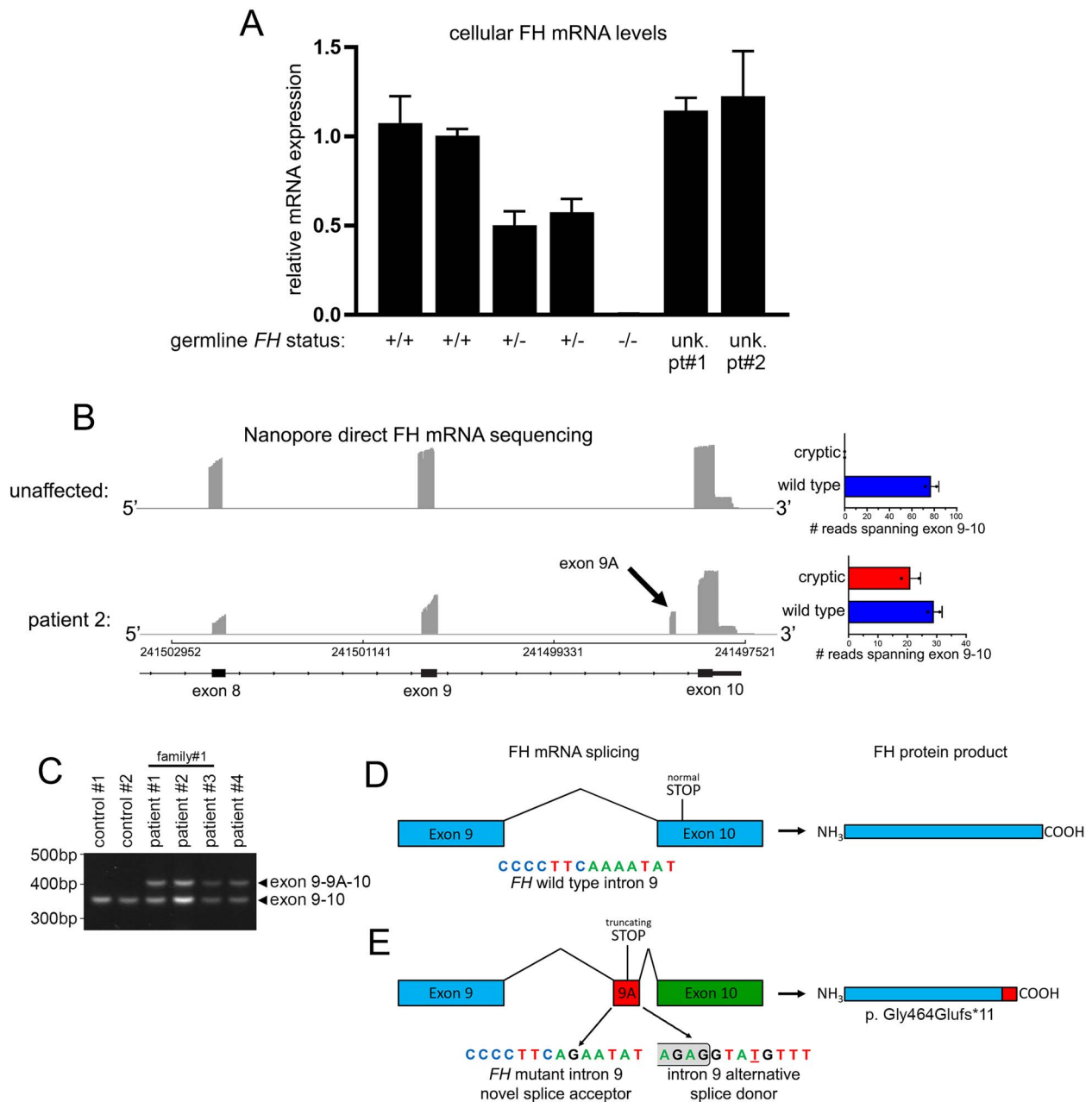
Figure 4. Analysis of *FH* mRNA in HLRCC-phenotypic patients. (**A**) *FH* mRNA expression levels were assessed by TaqMan qPCR and normalized to *MDH1* mRNA expression levels in cultured primary dermal fibroblasts obtained from two unaffected patients (FH$^{+/+}$), two known HLRCC patients harboring R343X and A101X *FH* mutations, respectively (FH$^{+/-}$), UOK348 tumor cells harboring compound heterozygous K371X and F191LX11 *FH* mutations (FH$^{-/-}$), and Patients #1 and #2. (**B**) *FH* mRNA sequences obtained by direct Nanopore total mRNA sequencing of Patient #2 and control unaffected patient fibroblast RNA were aligned to the human genome (see Results). (**C**) RT-PCR using primers flanking *FH* exons 9 and 10 was performed on fibroblast mRNA obtained from all three affected patients as well as a fourth unrelated patient. (**D**) Schematic diagram demonstrating the normal splicing between exons 9 and 10 of *FH* mRNA. (**E**) Impact of *FH* intron 9 chr1:241498239 T/C mutation on splicing and protein translation of *FH* mRNA. The resulting A/G base substitution in *FH* mRNA creates a strong splice acceptor site leading to retention of intron 9 sequence, and an alternative splice donor site 83 bp downstream from the mutation facilitates splicing with exon 10. The result is altered C-terminal amino acid incorporation and premature termination of the FH protein.

present downstream is utilized to produce a retained exon in the mutant *FH* mRNA, termed exon 9A.

LOH and immunohistochemical analyses of patient-derived tumors

Given our new understanding of the molecular nature of the *FH* variant present in this cohort of HLRCC patients, we undertook sequencing and histological analyses to test for signs of FH deficiency in patient-derived uterine and dermal leiomyoma specimens. Loss of heterozygosity (LOH) of the wild-type *FH* allele is frequently observed in FH-deficient leiomyomas and renal tumors (25–27). We sequenced the region of *FH* intron 9 containing the 1:241498239 T/C alteration in genomic DNA obtained from histological sections of two uterine leiomyoma specimens obtained from Patient #3. Our results revealed that both tumor specimens exhibited loss of the wild-type *FH* allele

(Fig. 5A). Next, we performed immunohistochemistry to examine FH protein levels in a uterine leiomyoma from Patient #3 and found that FH staining was negative in the tumor, whereas endothelial cells (white arrowhead) present within the tumor retained FH expression (Fig. 5B and C). These data suggest that the truncated FH protein produced by *FH* mRNA transcripts containing *FH* exon 9A was unstable *in vivo*. Proteins in FH-deficient tumors undergo covalent modification of cysteine residues forming an S-(2-succinyl)-cysteine (2-SC) protein adduct (10). Tumor cells in Patient #3's leiomyoma were strongly positive for the 2SC modification (Fig. 5D and E), while endothelial cells were 2SC-negative (Fig. 5E; white arrowhead). We also evaluated a dermal leiomyoma obtained from Patient #4, who is unrelated to Patients #1–3. We found that, whereas normal cells associated with a hair follicle in the specimen retained FH staining (Fig. 5F; white arrowhead), tumor cells in the section were FH-negative (Fig. 5F; black arrowheads). In contrast, normal cells in the skin biopsy were negative for 2SC staining (Fig. 5G; white arrowhead) while tumor cells were 2SC-positive (Fig. 5G; black arrowheads). These data confirmed that the leiomyoma specimens from patients in both families evaluated lost functional FH protein expression and accumulated fumarate, leading to positive 2SC immunoreactivity.

Discussion

While relatively rare, the prevalence of undiagnosed HLRCC cases is of concern. The need for timely germline *FH* genetic testing and interval screening of individuals who are at risk for developing FH-deficient RCC is clear (28–31). Sensitive and specific clinical genetic testing is crucial for accurate diagnosis of HLRCC and for testing of additional family members of affected individuals. Intronic variations are more difficult to detect because most current CLIA-certified genetic tests focus on the exons of disease genes, and intronic sequences are inherently less conserved than exon sequences, making it more difficult to predict the pathogenicity of intronic point mutations (32).

In this study, we evaluated patients from two independent families with clinical manifestations of HLRCC including uterine and dermal leiomyomas, but for whom standard clinical genetic testing revealed no phenotypic variations in the *FH* gene. We undertook functional biochemical and molecular analyses in normal tissues derived from these patients, starting with assessment of FH enzymatic activity, FH protein levels, *FH* mRNA levels, *FH* mRNA sequence analysis, and finally whole genome analysis to conclude that a single deep intronic point mutation is responsible for manifestations of HLRCC syndrome in these patients. This study underscores the utility of enzymatic assay in assessing FH function in individuals suspected to harbor germline alterations in the *FH* gene and highlights the usefulness of direct unbiased nanopore mRNA sequencing in revealing functional alterations in cellular mRNA splicing.

Cellular pre-mRNAs undergo splicing during and after transcription in the nucleus of the cell by the ribonucleoprotein spliceosome complex. DNA mutations resulting in the retention of cryptic exons in mature mRNAs most frequently arise from formation of a novel intronic donor splice site and activation of a pre-existing acceptor splice site (32), as was the case for a deep intronic mutation in the β-globin gene in a cohort of β-thalassemia patients (33). Less frequently, cryptic exon retention can result from formation of a novel splice acceptor site, as is the case with our novel HLRCC patients described in the present work. In either case, cryptic exon retention most

frequently results in creation of a premature stop codon in the mature mRNA, resulting in rapid nonsense-mediated mRNA decay (NMD) (34). We did not observe evidence for NMD in our patients, as total levels of *FH* mRNA were not decreased relative to controls, and ~50% of cellular *FH* mRNAs in the patients contained the retained exon 9A. The absence of NMD in our patients is consistent with the fact that the protein-truncating stop codon in the mutant *FH* exon 9A is located just 25 nucleotides upstream of the junction with the final exon of the mRNA (35).

At least two classes of pathogenic *FH* variants are known to exist in humans. One class of *FH* variants causes autosomal dominant inheritance of HLRCC, including point mutations, truncating frameshift mutations, and partial or complete deletions of the *FH* gene, all of which are thought to completely abrogate the enzymatic function of the affected *FH* allele. In contrast, certain germline homozygous or compound heterozygous *FH* mutations in humans can result in the autosomal recessive metabolic disorder fumarase deficiency, in which residual FH enzymatic activity in patient tissues is extremely low but not always undetectable (36,37), and there is evidence that not all fumarase deficiency *FH* allele carriers are at risk for development of HLRCC-related neoplasms (38,39). Thus, while bi-allelic deletion of the *FH* gene results in early embryonic lethality in mice (40), inheritance of either two low functioning *FH* alleles or inheritance of one low-functioning *FH* allele and one HLRCC-causing *FH* allele in humans can cause fumarase deficiency (39,41). We conclude that the 1:241498239 T/C alteration in the DNA of the patients evaluated in our study results in complete alternative mRNA splicing to form the stable, non-functional *FH* mRNA from the mutant allele, with no amount of normally spliced *FH* mRNA arising from this allele. Interestingly, the *FH* mutation discovered to cause HLRCC in our study was reported in one patient affected by fumarase deficiency (42), suggesting that the other affected *FH* allele in this patient (1078C > T; H402Y) must retain some amount of enzyme activity and thus be restricted to recessive inheritance of fumarase deficiency. Finally, given the genomic, biochemical, and histological data presented in this work, we believe that the 1:241498239 T/C *FH* alteration can be classified as a PVS1 null-variant *FH* allele according to the ACMG criteria (43,44), and that this allele is causative of both HLRCC and fumarase deficiency.

In addition to representing a new *FH* variant for genetic screening of patients suspected to be affected by HLRCC, the novel pathogenic *FH* variant identified in this work should also be considered in the context of screening for sporadic FH-deficient tumors. Disease-causing intronic mutations have been described in numerous inherited human disorders (45), including somatic occurrences in cancers (46). Recent advances have led to the introduction of clinically active, FDA-approved mRNA-based antisense oligonucleotide therapies for several human disorders (47). In contrast to protein-coding point mutations or deletions in the *FH* gene, the disease-causing 1:241498239 T/C *FH* alteration relies on the cellular splicing machinery to render a non-functional *FH* mRNA and protein. Thus, the concept of a targeted antisense oligonucleotide approach to restore even trace amounts of normal *FH* mRNA splicing from this mutant *FH* allele could constitute a patient-specific disease prevention strategy that does not rely on alteration of the cellular genome. Moreover, given that restoration of FH activity in cultured FH-deficient tumor cells reduced their invasiveness and abrogated tumor xenograft formation (48–50), restoration of FH activity in *FH*-deficient tumors harboring the 1:241498239 T/C *FH* alteration
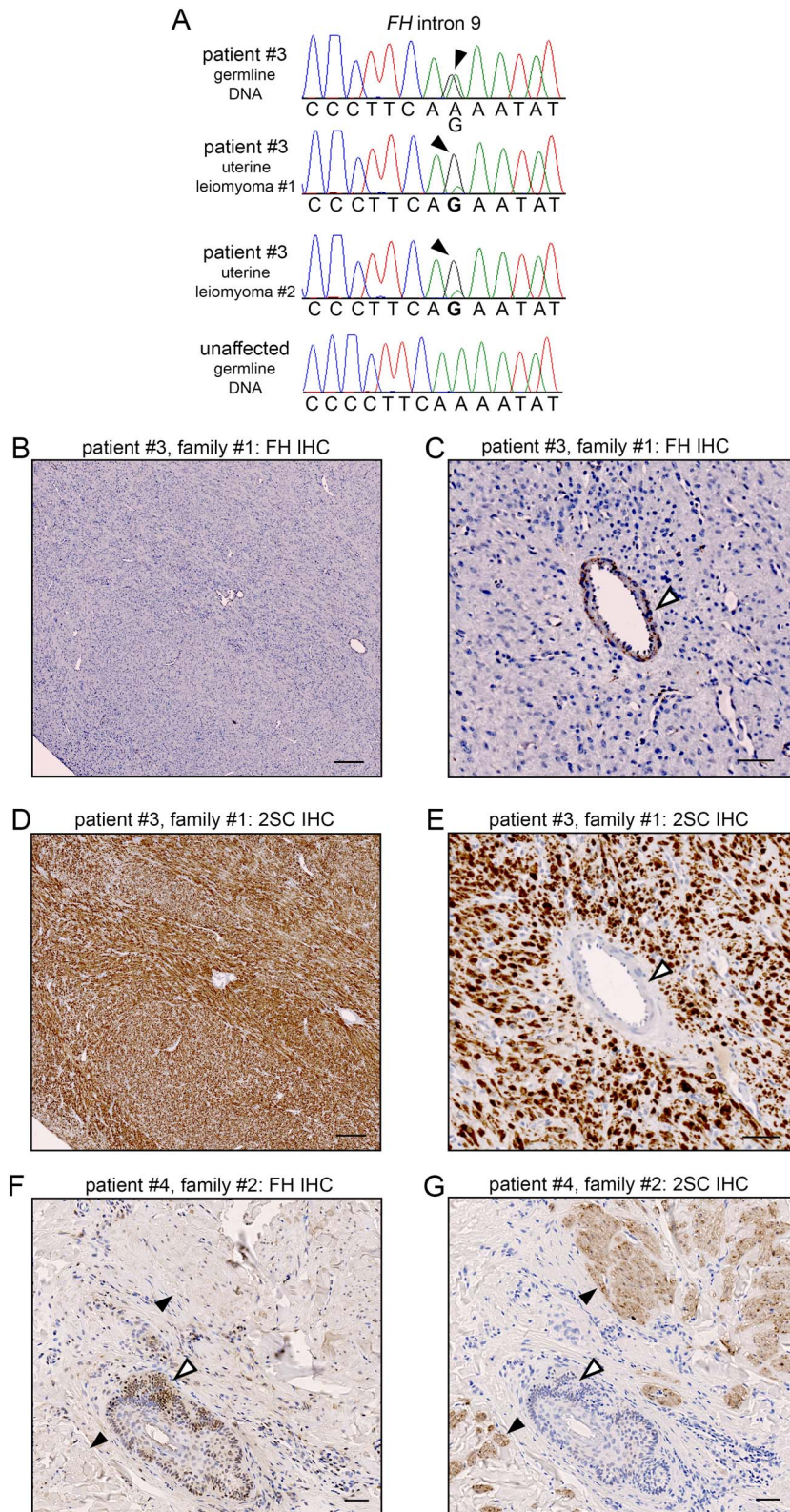
Figure 5. Genomic DNA sequencing and immunohistochemistry of uterine and dermal leiomyomata. (**A**) Heterozygous chr1:241498239 T/C mutation in *FH* intron 9 was verified by Sanger sequencing of the *FH* genomic negative strand in germline DNA obtained from Patient #3 (top chromatogram). Uterine leiomyomata obtained from Patient #3 during hysterectomy showed loss of the wild-type *FH* intron 9 allele (middle chromatograms). Unaffected germline DNA was included as a control (bottom chromatogram). (**B**) Immunohistochemical analysis of FH protein expression in a uterine leiomyoma obtained from Patient #3 revealed that FH protein staining was absent in the tumor cells. (**C**) Higher magnification images showed absent FH protein staining in tumor cells whereas blood vessel cells were positive for FH protein. (**D**) Positive immunoreactivity for 2SC was observed in the same uterine leiomyoma specimen. (**E**) Strong 2SC staining was observed in tumor cells, whereas blood vessel cells did not show 2SC immunoreactivity. (**F**) Dermal leiomyoma obtained from Patient #4 (Family #2) revealed absent FH protein expression in tumor regions (black arrowhead), whereas the same regions were positive for 2SC (**G**). In contrast, hair follicle cells in the middle of the specimen stained positive for FH and negative for 2SC (white arrowhead). Scale bar in B, D = 200 μm, C, E–G = 50 μm.

may provide a mutation-specific antiproliferative therapeutic strategy.

Supplementary Material

Funding

References

1. Grubb RL, Franks ME, Toro J *et al*. Hereditary leiomyomatosis and renal cell cancer: a syndrome associated with an aggressive form of inherited renal cancer. *J Urol* 2007;**177**: 2074–80.

2. Menko FH, Maher ER, Schmidt LS *et al*. Hereditary leiomyomatosis and renal cell cancer (HLRCC): renal cancer risk, surveillance and treatment. *Familial Cancer* 2014;**13**:637–44.

3. Wei MH, Toure O, Glenn GM *et al*. Novel mutations in FH and expansion of the spectrum of phenotypes expressed in families with hereditary leiomyomatosis and renal cell cancer. *J Med Genet* 2006;**43**:18–27.

4. Pithukpakorn M, Wei MH, Toure O *et al*. Fumarate hydratase enzyme activity in lymphoblastoid cells and fibroblasts of individuals in families with hereditary leiomyomatosis and renal cell cancer. *J Med Genet* 2006;**43**:755–62.

5. Pollard PJ, Briere JJ, Alam NA *et al*. Accumulation of Krebs cycle intermediates and over-expression of HIF1alpha in tumours which result from germline FH and SDH mutations. *Hum Mol Genet* 2005;**14**:2231–9.

6. Isaacs JS, Jung YJ, Mole DR *et al*. HIF overexpression correlates with biallelic loss of fumarate hydratase in renal cancer: novel role of fumarate in regulation of HIF stability. *Cancer Cell* 2005;**8**: 143–53.

7. Sullivan LB, Gui DY and Vander Heiden MG Altered metabolite levels in cancer: implications for tumour biology and cancer therapy. *Nat Rev Cancer* 2016;**16**:680–93.

8. Linehan WM, Spellman PT, Ricketts CJ *et al*. Comprehensive molecular characterization of papillary renal cell carcinoma. *N Engl J Med* 2016;**374**:135–45.

9. Ricketts CJ, Killian JK, Vocke CD *et al*. Kidney tumors associated with germline mutations of FH and SDHB show a CpG island methylator phenotype (CIMP). *PLoS One* 2022;**17**:1–21.

10. Bardella C, El-Bahrawy M, Frizzell N *et al*. Aberrant succination of proteins in fumarate hydratase-deficient mice and HLRCC patients is a robust biomarker of mutation status. *J Pathol* 2011;**225**:4–11.

11. Linehan WM, Schmidt LS, Crooks DR *et al*. The metabolic basis of kidney cancer. *Cancer Discov* 2019;**8**:1006–21.

12. Crooks DR, Maio N, Lang M *et al*. Mitochondrial DNA alterations underlie an irreversible shift to aerobic glycolysis in fumarate hydratase-deficient renal cancer. *Sci Signal* 2021;**14**: 1–18.

13. Kulkarni RA, Bak DW, Wei D *et al*. A chemoproteomic portrait of the oncometabolite fumarate. *Nat Chem Biol* 2019;**15**:391–400.

14. Yang M, Ternette N, Su H, *et al*. (2014) The succinated proteome of FH-mutant tumours. *Meta*, **4**, 640–54.

15. Mannan R, Wang X, Bawa PS *et al*. Characterization of protein S-(2-succino)-cysteine (2SC) succination as a biomarker for fumarate hydratase-deficient renal cell carcinoma. *Hum Pathol* 2023;**134**:102–13.

16. Gupta S, Swanson AA, Chen YB *et al*. Incidence of succinate dehydrogenase and fumarate hydratase-deficient renal cell carcinoma based on immunohistochemical screening with SDHA/SDHB and FH/2SC. *Hum Pathol* 2019;**91**:114–22.

17. Chen YB, Brannon AR, Toubaji A *et al*. Hereditary leiomyomatosis and renal cell carcinoma syndrome-associated renal cancer: recognition of the syndrome by pathologic features and the utility of detecting aberrant succination by immunohistochemistry. *Am J Surg Pathol* 2014;**38**:627–37.

18. Vocke CD, Ricketts CJ, Merino MJ *et al*. Comprehensive genomic and phenotypic characterization of germline FH deletion in hereditary leiomyomatosis and renal cell carcinoma. *Genes Chromosomes Cancer* 2017;**56**:484–92.

19. Gardie B, Remenieras A, Kattygnarath D *et al*. Novel FH mutations in families with hereditary leiomyomatosis and renal cell cancer (HLRCC) and patients with isolated type 2 papillary renal cell carcinoma. *J Med Genet* 2011;**48**:226–34.

20. Kulkarni RA, Briney CA, Crooks DR *et al*. Photoinducible Oncometabolite detection. *Chembiochem* 2019;**20**:360–5.

21. Lanfear R, Schalamun M, Kainer D *et al*. MinIONQC: fast and simple quality control for MinION sequencing data. *Bioinformatics* 2019;**35**:523–5.

22. Robinson JT, Thorvaldsdottir H, Winckler W *et al*. Integrative genomics viewer. *Nat Biotechnol* 2011;**29**:24–6.

23. Ricketts CJ, Vocke CD, Lang M *et al*. A germline 1;3 translocation disrupting the VHL gene: a novel genetic cause for von Hippel-Lindau. *J Med Genet* 2022;**59**:18–22.

24. Zengeya TT, Garlick JM, Kulkarni RA *et al*. Co-opting a bioorthogonal reaction for Oncometabolite detection. *J Am Chem Soc* 2016; **138**:15813–6.

25. Sanz-Ortega J, Vocke C, Stratton P *et al*. Morphologic and molecular characteristics of uterine leiomyomas in hereditary leiomyomatosis and renal cancer (HLRCC) syndrome. *Am J Surg Pathol* 2013;**37**:74–80.

26. Launonen V, Vierimaa O, Kiuru M *et al*. Inherited susceptibility to uterine leiomyomas and renal cell cancer. *Proc Natl Acad Sci U S A* 2001;**98**:3387–92.

27. Toro JR, Nickerson ML, Wei MH *et al*. Mutations in the fumarate hydratase gene cause hereditary leiomyomatosis and renal cell cancer in families in North America. *Am J Hum Genet* 2003;**73**: 95–106.

28. Palma CA, Watson G, Earls P *et al*. A novel case of hereditary leiomyomatosis- associated renal cell carcinoma with metastasis to pituitary gland. *Urol Case Rep* 2022;**45**:102206.

29. Catarina T, Quental MS, Brandao JR *et al*. Hereditary Leiomyomatosis and renal cell cancer-recognizing patterns may save lives. *J Kidney Cancer VHL* 2022;**9**:27–31.

30. Yu Y, Zheng M, Zhu W *et al*. Hereditary leiomyomatosis and renal cell cancer (HLRCC): case series and review of the literature. *Urol Oncol* 2021;**39**:791.e9–e16.

31. Young KZ, Raisanen TD, Else T *et al*. A few pink papules in an adult woman: incidental finding leads to diagnosis of hereditary

leiomyomatosis and renal cell cancer. *JAAD Case Rep* 2019;**5**: 419–21.

32. Vaz-Drago R, Custodio N and Carmo-Fonseca M Deep intronic mutations and human disease. *Hum Genet* 2017;**136**: 1093–111.

33. Dobkin C, Pergolizzi RG, Bahre P *et al*. Abnormal splice in a mutant human beta-globin gene not at the site of a mutation. *Proc Natl Acad Sci U S A* 1983;**80**:1184–8.

34. Popp MW and Maquat LE Organizing principles of mammalian nonsense-mediated mRNA decay. *Annu Rev Genet* 2013; **47**:139–65.

35. Nagy E and Maquat LE A rule for termination-codon position within intron-containing genes: when nonsense affects RNA abundance. *Trends Biochem Sci* 1998;**23**:198–9.

36. Zinn AB, Kerr DS and Hoppel CL Fumarase deficiency: a new cause of mitochondrial encephalomyopathy. *N Engl J Med* 1986;**315**:469–75.

37. Rustin P, Bourgeron T, Parfait B *et al*. Inborn errors of the Krebs cycle: a group of unusual mitochondrial diseases in human. *Biochim Biophys Acta* 1997;**1361**:185–97.

38. Zhang L, Walsh MF, Jairam S *et al*. Fumarate hydratase FH c.1431_1433dupAAA (p.Lys477dup) variant is not associated with cancer including renal cell carcinoma. *Hum Mutat* 2020;**41**: 103–9.

39. Kamihara J, Horton C, Tian Y *et al*. Different fumarate hydratase gene variants are associated with distinct cancer phenotypes. *JCO Precis Oncol* 2021;**5**:1568–78.

40. Pollard PJ, Spencer-Dene B, Shukla D *et al*. Targeted inactivation of fh1 causes proliferative renal cyst development and activation of the hypoxia pathway. *Cancer Cell* 2007;**11**:311–9.

41. Peetsold M, Goorden S, Breuning M *et al*. Fumarase deficiency: a case with a new pathogenic mutation and a review of the literature. *J Child Neurol* 2021;**36**:310–23.

42. Allegri G, Fernandes MJ, Scalco FB *et al*. Fumaric aciduria: an overview and the first Brazilian case report. *J Inherit Metab Dis* 2010;**33**:411–9.

43. Walker LC, Hoya M, Wiggins GAR *et al*. Using the ACMG/AMP framework to capture evidence related to predicted and observed impact on splicing: recommendations from the ClinGen SVI splicing subgroup. *Am J Hum Genet* 2023;**110**:1046–67.

44. Abou Tayoun AN, Pesaran T, DiStefano MT *et al*. Recommendations for interpreting the loss of function PVS1 ACMG/AMP variant criterion. *Hum Mutat* 2018;**39**:1517–24.

45. Scotti MM and Swanson MS RNA mis-splicing in disease. *Nat Rev Genet* 2016;**17**:19–32.

46. Jung H, Lee KS and Choi JK Comprehensive characterisation of intronic mis-splicing mutations in human cancers. *Oncogene* 2021;**40**:1347–61.

47. Damase TR, Sukhovershin R, Boada C *et al*. The limitless future of RNA therapeutics. *Front Bioeng Biotechnol* 2021;**9**:628137.

48. Sourbier C, Ricketts CJ, Matsumoto S *et al*. Targeting ABL1-mediated oxidative stress adaptation in fumarate hydratase-deficient cancer. *Cancer Cell* 2014;**26**:840–50.

49. Tong WH, Sourbier C, Kovtunovych G *et al*. The glycolytic shift in fumarate-hydratase-deficient kidney cancer lowers AMPK levels, increases anabolic propensities and lowers cellular iron levels. *Cancer Cell* 2011;**20**:315–27.

50. Fitzsimmons CM, Lunger JC, Chan D *et al*. Rewiring of RNA methylation by the oncometabolite fumarate in renal cell carcinoma. *bioRxiv* 2023; in press.